Cubane Dimerization: Cu4 vs Cu8 Copper Iodide Clusters

Raquel Utrera Melero, Marie Cordier, Florian Massuyeau, Jean-Yves Mevellec, Aydar Rakhmatullin, Charlotte Martineau-Corcos, Camille Latouche, Sandrine Perruchas

Cubane dimerization: Cu_4 *vs.* Cu_8 copper iodide clusters

Raquel Utrera-Melero,[a] Marie Cordier,[b] Florian Massuyeau,[a] Jean-Yves Mevellec,[a] Aydar Rakhmatullin,[c] Charlotte Martineau-Corcos,[c,d,e] Camille Latouche,[a] and Sandrine Perruchas[a]**

[a] Nantes Université, CNRS, Institut des Matériaux de Nantes Jean Rouxel, IMN, F-44000 Nantes, France.
Phone: (+33) (0)2 40 37 63 35. E-mail: sandrine.perruchas@cnrs-imn.fr, camille.latouche@cnrs-imn.fr.

[b] Univ. Rennes, CNRS, ISCR (Institut des Sciences Chimiques de Rennes) - UMR 6226, F-35000 Rennes, France.

[c] CEMHTI-CNRS, UPR 3079, 1D avenue de la recherche scientifique, 45071 Orléans Cedex 2, France.

[d] MIM, Institut Lavoisier de Versailles (ILV), UMR CNRS 8180, Université de Versailles St-Quentin en Yvelines (UVSQ), 45, avenue des Etats-Unis, 78035 Versailles Cedex, France.

[e] current address: CortecNet, 7 avenue du Hoggar, 91940 Les Ulis, France.

Abstract.

Copper(I) halides are well known for their structural diversity and rich photoluminescence properties, showing great potential for the development of solid-state lighting technology. A series of four molecular copper iodide clusters based on the $[Cu_4I_4]$ cubane geometry is reported. Among them, $[Cu_8I_8]$ octanuclear clusters of rare geometry resulting from the dimerization of the tetranuclear counterparts were also synthesized. Two different phosphine ligands were studied, bearing either a styrene or an ethyl group. Therefore, the effect of the dimerization and of the ligand nature on the photophysical properties of the resulting clusters is investigated. The structural differences were analysed by single crystal X-Ray diffraction (SCXRD), solid-state NMR (Nuclear magnetic Resonance), Infrared, and Raman analyses. Comparatively to the ethyl group, the styrene function appears to greatly impact the photophysical properties of the clusters. The luminescence thermochromic properties of the ethyl derivatives and the intriguing photophysical properties of the clusters with styrene function were rationalized by density functional theory (DFT) calculations. Thus, the styrene group significantly lowers in energy the vacant orbitals and consequently affects the global energetic layout of the clusters. From this study, the nuclearity of the copper iodide clusters has eventually less influence on the photophysical properties than the nature of the ligand. The design of proper ligands should therefore be considered when developing materials for specific lighting applications.

Keywords. copper iodide cluster, cubane structure, cluster dimerization, photoluminescence, luminescence thermochromism.

Introduction.

To develop environmentally friendly and sustainable solid-state luminescent materials, intense research on materials free of rare earth and lead ions is currently being carried out.[1–5] Due to the accessibility of elemental copper and the remarkable photophysical properties of copper(I) complexes,[6–9] Cu(I)-based materials are especially interesting for the development of cost-effective emissive materials that also combine high efficiency with low toxicity.[10–13] Among the Cu(I) compounds, the family of copper halides is characterized by a wide range of photophysical properties associated to a large structural diversity.[14–17] In particular, copper iodide compounds display intense and stable photoluminescence properties, making them a relevant alternative to lead-based hybrid perovskites.[18–23]

Multinuclear copper(I) iodide complexes or molecular clusters having more than two copper atoms, offer a large range of photophysical properties thanks to their various possible optical transitions, which is of particular interest for developing light-emitting stimuli-responsive materials.[24–30] Indeed, the interplay between different transitions (Metal-to-Ligand Charge Transfer MLCT, Halide-to-Ligand Charge Transfer XLCT, Metal-Metal MM…) can lead to competitive excited states and sensitivity to external factors. For instance, luminescence thermochromism can be observed when excited states are thermally coupled.[31–34] TADF (Thermally Activated Delayed Fluorescence) process may also be involved in some cases.[35,36] The metallophilic interactions that may be present in these compounds can also be responsible for luminescent mechanochromic properties.[37,38] Because of the adaptability of the d^{10} electronic configuration of Cu(I) and the various coordination modes of halides, multinuclear copper(I) iodide complexes present diverse nuclearities and geometries features.[39–41] The small energy difference between different structures having similar coordination numbers further adds to the structural diversity of these compounds, as illustrated by the tendency towards crystalline polymorphism.[42–44] Among the many multinuclear copper(I) iodide complexes existing, the tetranuclear cluster formulated $[Cu_4I_4L_4]$ (L = organic ligand) based on the cubane geometry is by far the best known because of its multistimuli-responsive photoluminescent properties.[45,41] In addition to the previously cited luminescence thermochromic and mechanochromic properties, solvatochromism[46–49] and even rigidochromism[50,51] can be displayed. Therefore, promising applications are expected in the domain of emitting devices.[52–57] In this context, molecular clusters of high nuclearity favouring multiple cuprophilic interactions while preserving the cubane geometry are particularly interesting to get original photophysical properties. Such compounds may offer many applicative perspectives as multifunctional light-emitting solid-state materials.

Here, we report on the study of a series of four molecular copper iodide clusters based on the $[Cu_4I_4]$ multimetallic core of cubane geometry coordinated by phosphine ligands. In addition to the tetranuclear clusters, the formation of dimerized $[Cu_8I_8]$ octanuclear clusters is presented. The ligands are based on triphenylphosphine bearing a styrene function. Because this styrene function appears to greatly impact the photophysical properties of the clusters, another ligand for which the styrene group was replaced by an ethyl chain, was studied comparatively. The synthesis, structural and photophysical characterisations of these four copper iodide clusters are presented. The structural differences were analysed by single crystal X-Ray diffraction (SCXRD), solid-state NMR, IR, and Raman analyses. The luminescence thermochromic properties of the ethyl derivatives and the intriguing photophysical properties of the clusters with styrene function were rationalized by density functional theory (DFT) calculations. This study permit to evaluate the effect that the nature of the ligands and the nuclearity of copper iodide metal center can have on the photophysical properties of the resulting clusters.

Results and Discussions.

Synthesis and crystal structures.

The four clusters were synthesized in solution by reacting CuI with the phosphine ligands. The styrene phosphine formulated $Ph_2P(C_6H_4)CH{=}CH_2$ is commercially available whereas the ethyl derivative $Ph_2P(C_6H_4)CH_2CH_3$ was synthesized by lithiation of the bromoethylbenzene and reaction with chlorodiphenylphosphine (experimental details in SI). The nomenclature of the four different clusters obtained is reported in Figure 1. Upon recrystallization of the complexes, the monomer $[Cu_4I_4L_4]$ (**M**) and the dimer $[Cu_8I_8L_6]$ (**D**) illustrated in Figure 1, formed concomitantly in the case of the two different ligands. Changing the CuI:L stoichiometry or the solvents nature gave similar results. Crystals of the monomers and the dimers present distinguishable morphologies. While the monomers form needles, the dimers has rhomboid bulky shape (Figure S1). For the styrene phosphine, the two compounds (**C-StyM** and **C-StyD**) were separated manually under an optical microscope. In the case of the ethyl phosphine, pure $[Cu_8I_8L_6]$ (**C-EthylD**) could be obtained exclusively at the first stage of the crystallization, the monomer (**C-EthylM**) forming afterwards. Elemental analysis results are in accordance with the clusters formula and indicate absence of solvent trapped in the crystalline powders (SI).

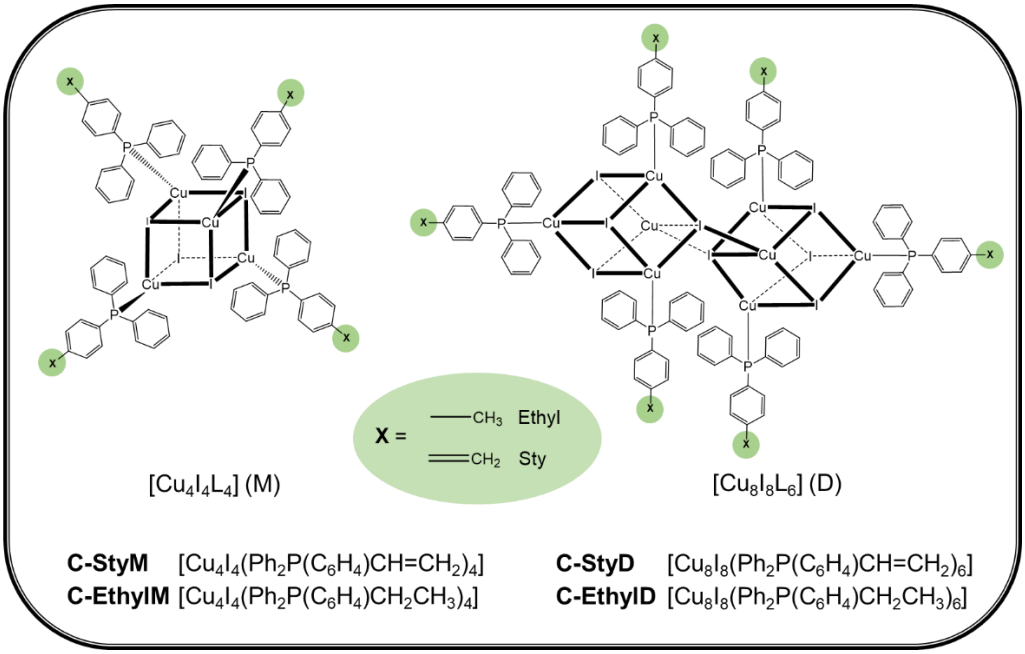

Figure 1. Schematic drawing of the $[Cu_4I_4L_4]$ (Monomer) and $[Cu_8I_8L_6]$ (Dimer) clusters (L = phosphine ligand with ethyl or styrene group) and labels of the studied compounds.

Single crystals suitable for SCXRD analyses could be obtained for the two $[Cu_8I_8L_6]$ dimers, **C-StyD** and **C-EthylD** and for the $[Cu_4I_4L_4]$ styrene monomer **C-StyM**. The crystalline needles of **C-EthylM** were too thin for collecting accurate data. Experimental crystallographic details and data are reported in SI. **C-StyM** crystallizes in the *P* $2_1/n$ and presents the $[Cu_4I_4L_4]$ cluster cubane structure as shown in Figure 2. There are two crystallographically independent clusters in this structure (C-StyM*a* and C-StyM*b*) having very similar geometric characteristics. One styrene group of each cluster and one phenyl group for C-StyM*b* are disordered over two positions (Figure S3). The Cu atoms are all in the pseudo-tetrahedral I_3CuP coordination geometry. Selected distances and angles are listed in Table 1. The volume of the two Cu_4 tetrahedra are therefore very close (3.06 and 2.98 $Å^3$) but from comparison of the I-Cu-I angles, the cluster core in C-StyM*b* is more symmetrical than that of C-StyM*a* (standard deviation of

4.11° *vs* 2.52°, respectively). The Cu-I, Cu-P distances as well as I-Cu-I angles for **C-StyM** are all in the range of values reported for cubane copper iodide clusters coordinated by phosphine ligands (Table 1).[54,58,59] This is also the case for the Cu-Cu distances which are close to the van der Waals interaction value of 2.8 Å.[60] The crystalline packing of **C-StyM** can be described as rows of clusters running along the *b* axis (Figure 2). No π-π stacking between the phenyl groups is observed.

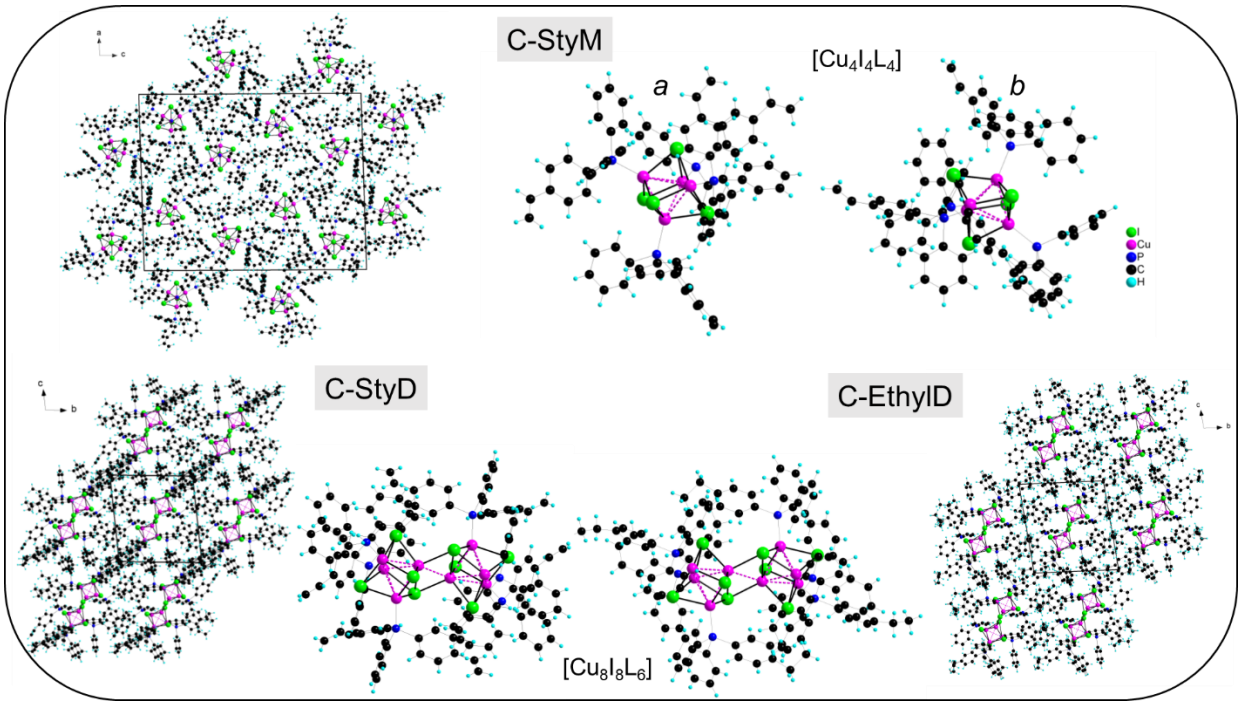

Figure 2. Crystal and molecular structures of **C-StyM** with two independent (*a* and *b*) $[Cu_4I_4L_4]$ clusters and of **C-StyD** and **C-EthylD** $[Cu_8I_8L_6]$ clusters. Cu-Cu contacts are shown in dashed pink lines. Disorder on the ligands is not shown for clarity.

C-StyD and **C-EthylD** crystallize in the triclinic *P* -1 space group and are isostructural (Figure S2). They present dimerized $[Cu_8I_8]$ clusters resulting from two $[Cu_4I_4]$ units linked through one cube edge by two Cu-I bonds. This 'double cubane' structure has an inversion center located in the middle of the connection forming a rhomboid $[Cu_2I_2]$ motif (Figure 2). The ligands are also disordered in **C-StyD** and **C-EthylD** involving the $C{=}CH_2$ and CH_2CH_3 moieties as well as the phenyl groups (Figure S4). In this dimerized cubane structure, the Cu atoms present a I_3CuP coordination geometry as in the monomer but also the CuI_4 pseudo-tetrahedral geometry for two Cu atoms involved in the connection. The cubane entity in **C-StyD** and **C-EthylD** present very close Cu-I (2.678 *vs* 2.683 Å) and Cu-P distances (2.251 *vs* 2.250 Å, respectively), and I-Cu-I angles (108.89 *vs* 108.91°), as reported in Table 1. The Cu-Cu mean distances within the cubane are quite similar for the two dimers (2.947 and 2.951 Å) and lie in the range of van der Waals values. The Cu_4 tetrahedra volume are also very close (2.99 *vs* 3.01 $Å^3$) having similar shape too (I-Cu-I angles standard deviation of 2.62 *vs* 2.49°, respectively). Therefore, there is no particular distortion of the cubane cluster due to the dimerization. In the $[Cu_2I_2]$ connection, the Cu-I and Cu-Cu distances are in the range of classical values. However, the longer Cu-I distances of **C-EthylD** induces longer Cu-Cu distances compared with **C-StyD** (2.9561(9) *vs* 3.060(3) Å). The crystalline packing of **C-StyD** and **C-EthylD** can be described as molecular plane (*ac)* of clusters. Intermolecular π-π stacking interactions between the phenyl groups are observed in the structures with interplanar distances in the 3.75-3.96 Å range (Figure S5).

PXRD (Powder X-Ray Diffraction) analysis confirm the purity and homogeneity of the compounds by comparison with the SCXRD data (Figure S6). **C-StyD** and **C-EthylD** present similar powder patterns as expected form their isostructurality, but are clearly distinct from those of the **C-StyM** and **C-EthylM** monomers.

The dimerized octanuclear $[Cu_8I_8L_6]$ motif is by far less common compared with the tetranuclear one in the copper iodide clusters with only four examples reported in the literature. Two of them are found in coordination polymers with the first one comprising both $[Cu_8I_8L_6]$ and hexagonal prismatic $[Cu_6I_6L_6]$ clusters with DABCO (1,4-diazabicyclo[2.2.2]octane) as bidentate nitrogen-based ligand[61,62] and the second one with a dithiother ligand.[63] Regarding discrete entities as in our case, only one example has a phosphine ligand, the other one being based on a sulfur ligand.[64] Compared with **C-StyD** and **C-EthylD**, the phosphine derivative formulated $[Cu_8I_8(4\text{-dpda})_6]$ (dpda = 4-(diphenylphosphineno)-N,N-dimethylaniline)[65] presents similar intramolecular geometric parameters (recorded at 113 K) which are in the range of copper iodide cubane clusters. It is interesting to note that in the case of the sulfur-based ligand, the tetranuclear monomer is also formed.[64]

Table 1. Selected bond lengths and angles from SCXRD data recorded at 150 K. *a* and *b* stand for the two independent clusters in the **C-StyM** structure.

	C-StyM		***C-StyD***	***C-EthylD***
	a	***b***	2.9561(9) *(intercubane)*	3.060(3) *(intercubane)*
***Cu-Cu** (Å)*	2.877(2)	2.826(2)		
	2.941(2)	2.840(2)	2.8404(6) x 2	2.982(2) x 2
	3.004(2)	2.916(2)	2.8554(6) x 2	2.865(2) x 2
	2.862(2)	2.958(2)	2.9070(7) x 2	2.893(2) x 2
	2.904(2)	3.009(2)	2.9909(7) x 2	3.102(2) x 2
	3.231(2)	3.094(2)	2.9814(7) x 2	3.036(2) x 2
			3.1036(7) x 2	2.828(2) x 2
mean	*2.970(2)*	*2.941(2)*	*2.947(1)*	*2.951(2)*
standard-deviation	*0.138*	*0.102*	*0.099*	*0.107*
Cu_4 ($Å^3$)	*3.06(1)*	*2.98(1)*	*2.99(1)* x 2	*3.01(2)* x 2
			2.7046(5) x 2 *(intercubane)*	2.7133(15) x 2 *(intercubane)*
***Cu-I** (Å)*				
	2.6562(14)	2.6546(17)	2.6469(5) x 2	2.6693(16) x 2
	2.6818(15)	2.6835(17)	2.7328(5) x 2	2.6784(16) x 2
	2.6919(15)	2.7018(18)	2.7556(5) x 2	2.6955(16) x 2
	2.6343(16)	2.6557(17)	2.6362(5) x 2	2.6395(16) x 2
	2.7135(16)	2.6809(16)	2.6515(5) x 2	2.6601(15) x 2
	2.7168(16)	2.7041(19)	2.6868(6) x 2	2.6957(16) x 2
	2.6698(14)	2.6746(16)	2.6691(5) x 2	2.6416(15) x 2
	2.6829(15)	2.7019(17)	2.6776(6) x 2	2.6632(15) x 2
	2.7131(17)	2.7207(18)	2.6870(5) x 2	2.7002(16) x 2
	2.6528(15)	2.6635(17)	2.6410(5) x 2	2.6535(15) x 2
	2.6878(16)	2.6847(19)	2.6538(5) x 2	2.7454(16) x 2
	2.7239(16)	2.7012(17)	2.6941(6) x 2	2.7558(16) x 2
mean	*2.6854(17)*	*2.6856(19)*	*2.6777(6)*	*2.6832(16)*
standard-deviation	*0.028*	*0.021*	*0.037*	*0.037*

***Cu-P** (Å)*	2.258(3) 2.259(3) 2.258(3) 2.255(3)	2.253(3) 2.266(3) 2.257(3) 2.264(4)	2.251(1) x 2 2.251(1) x 2 2.261(1) x 2	2.252(3) x 2 2.249(3) x 2 2.250(3) x 2
mean *standard-deviation*	*2.258(3)* *0.0017*	*2.260(4)* *0.0060*	*2.251(1)* *0.0001*	*2.250(3)* *0.0015*
***I-Cu-I** (°)*	108.87(5) 110.76(5) 108.31(5) 113.42(5) 108.97(5) 110.03(5) 111.24(5) 111.00(5) 99.69(5) 101.39(5) 111.86(5) 107.54(5)	112.50(6) 109.23(6) 111.19(6) 109.31(6) 111.95(6) 106.98(6) 109.27(6) 106.16(6) 109.15(6) 112.09(6) 107.83(6) 104.42(6)	103.163(17) x 2 104.692(17) x 2 112.947(18) x 2 *(intercubane)* 112.936(18) x 2 112.928(18) x 2 109.436(18) x 2 109.324(18) x 2 109.746(17) x 2 105.400(17) x 2 110.009(18) x 2 109.126(17) x 2 104.281(17) x 2 108.012(19) x 2 109.070(20) x 2 106.372(18) x 2	102.80(5) x 2 106.57(5) x 2 110.49(5) x 2 *(intercubane)* 109.23(5) x 2 106.91(5) x 2 106.96(5) x 2 109.80(5) x 2 109.56(5) x 2 105.26(5) x 2 110.39(6) x 2 112.84(5) x 2 113.09(5) x 2 108.26(5) x 2 108.98(5) x 2 105.69(5) x 2
mean *standard-deviation*	*108.59(5)* *4.11*	*109.17(6)* *2.52*	*108.89(2)* *2.62*	*108.91(5)* *2.49*

Solid-state Nuclear Magnetic Resonance (NMR).

The ^{63}Cu static NMR spectra of the four different clusters are presented in Figure 3. This nucleus has a large quadrupolar moment giving rise to broad spectra presenting overlapping individual contributions, even at high magnetic field.[66] Because four and eight nonequivalent Cu sites are present in the monomers and the dimers respectively, deconvolution of the patterns was not attempted. **C-StyM** and **C-EthylM** present two large patterns with chemical shifts ranging from 1000 to -900 ppm. This spectra have the characteristic shape of complexes of $[Cu_4I_4L_4]$ cubane geometry with the Cu atoms having all the I_3CuP coordination environment.[59,67] As example, rhomboid $[Cu_2I_2L_2]$ complexes present much larger quadrupolar coupling constants.[66] This constitutes an additional proof of the $[Cu_4I_4]$ monomer structure of **C-EthylM**. For the $[Cu_8I_8L_6]$ dimers clusters (**C-StyD** and **C-EthylD**), the shape of the spectra is clearly different with a larger width (1200 to -1500 ppm) having in this case three contributions. The two contributions belonging to the I_3CuP coordination mode can be easily identified and the one around 200 ppm can be attributed to the CuI_4 coordination mode existing between the two cubane moieties in the $[Cu_2I_2]$ connection. Similar signal was already reported for the $[Cu_6I_6(PPh_2(CH_2)_3PPh_2)_3]$ cluster of 'eared-cubane' geometry having CuI_4 coordination mode too.[68] The distinct ^{63}Cu NMR signatures of the monomer and the dimer clusters shows that this technique is very effective in identifying the molecular structure of copper halide compounds.

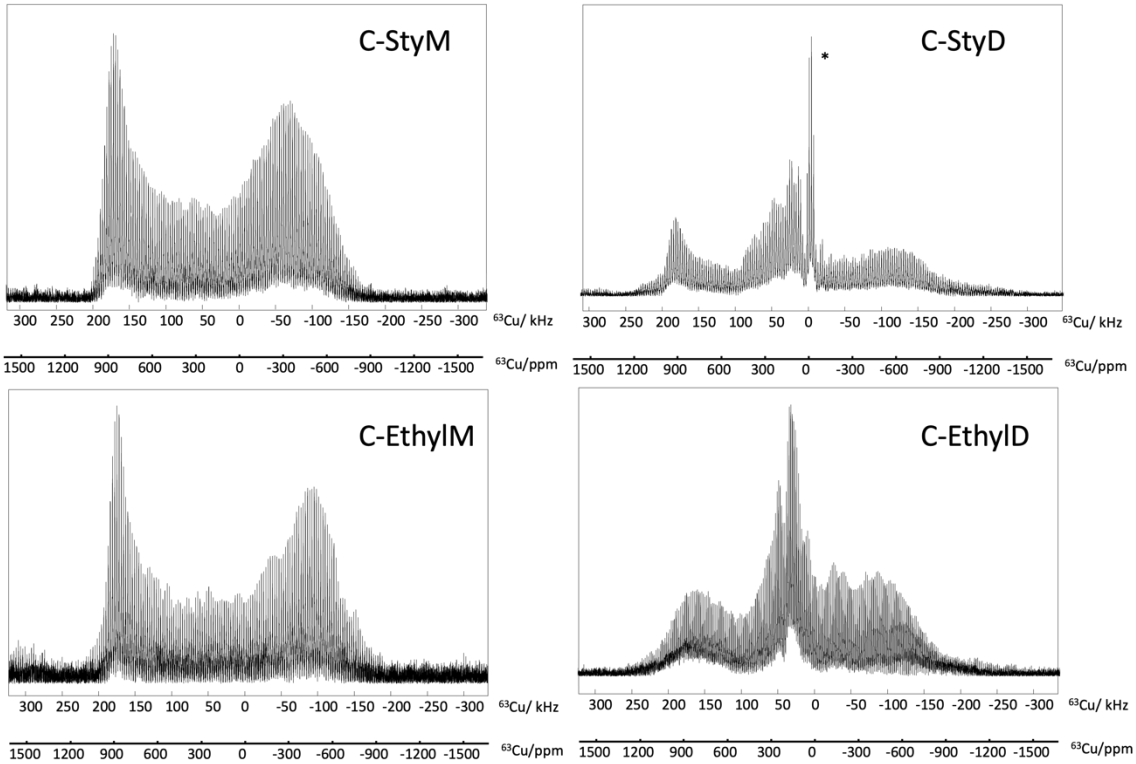

Figure 3. Solid-state NMR ^{63}Cu static WURST-QCPMG spectra of **C-Sty** and **C-Ethyl** clusters. The star indicates a parasite signal.

The ^{31}P CPMAS NMR spectra reported in Figure 4 are all centered between -20 and -25 ppm that is typical for such copper halide complexes of cubane geometry.[59,67,68] Whereas defined peaks can be observed for the dimers, broader features are found for the monomers. With eight independent phosphorus atoms in **C-StyM**, 16 quartets are expected due to the one-bond *J*-couplings between the ^{31}P and the two copper isotopes (^{65}Cu with 30.8 % natural abundance and ^{63}Cu with 69.2 % natural abundance) of both nuclear spin value of 3/2. Those quartets therefore highly overlap. The peaks are also not evenly spaced due to residual dipolar coupling.[69] Peak broadening is additionally due to the disorder of the ligand as detected in the SCXRD analysis. Precise contributions attribution is consequently prevented in this case. One can however notice less disorder (*i.e.* sharper peaks) for **C-EthylM**. For the dimers, the three independent phosphorus atoms lead to 6 quartets. The ^{31}P NMR spectrum can be greatly simplified by a ^{31}P-^{63}Cu J-HMQC MAS experiment, on which only the ^{31}P coupled to the central transition of the copper atoms with spin ^{63}Cu is retained.[70] For **C-StyD**, two different ^{31}P NMR resonances are found (Figure S7). The two doublets of 2:1 relative intensity are located at δ_{iso} = - 18.2 ppm ($^{1}J^{31P\text{-}63Cu}$ = 1597 Hz) and δ_{iso} = - 24.05 ppm ($^{1}J^{31P\text{-}63Cu}$ = 1231 Hz) which can be assigned to P1 (site multiplicity 48e) and P2 (site multiplicity 16c) in the structure, respectively. Unfortunately, the resolution on the ^{31}P-^{63}Cu *J*-HMQC MAS NMR spectrum of **C-StyM** is still low, despite the narrowing of the pattern, and no individual ^{31}P sites can be distinguished, as they have too close chemical shifts. The nature of the ligands and the nuclearity of the cluster core have thus no significant effect on the ^{31}P chemical shift values. Absence of ligand effect can be explained by the separation of the ethyl or styrene group from the phosphorus atom by a phenyl ring.

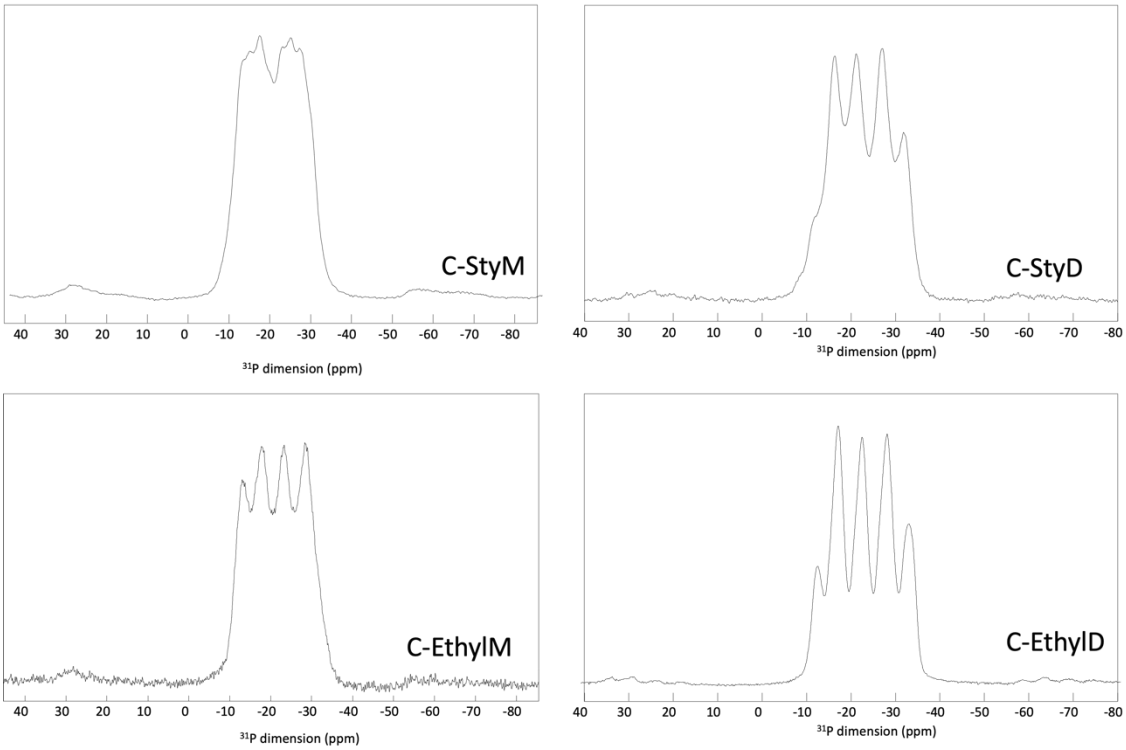

Figure 4. Solid-state ^{31}P CPMAS NMR spectra of **C-Sty** and **C-Ethyl** clusters.

Infrared (IR) and Raman spectroscopies.

The recorded IR and Raman spectra of the clusters are reported in Figures 5 and 6. Simulation of the spectra were carried out by DFT calculations (details in SI and below) and a relatively good match was obtained with the experiment upon correction of a scaling factor of 0.96 on the computed vibrational energies, as commonly used (Figures S8-11).[71] This good match allows us to suggest an assignment of the IR and Raman bands (Table S2-5) but it is worth noting the complexity of the assignment due to the large number of vibrational normal modes, which are in addition often entangled and coupled. In Figure 5 are presented the far-IR spectra (50-650 cm^{-1}) and the mid-IR one (400-4000 cm^{-1}). Above 200 cm^{-1}, the spectra are in the whole very similar for the clusters and the bands can be all attributed to ligand vibrations. Specific bands are observed for the styrene and ethyl groups for the clusters with the same ligand. At low frequencies, take place vibrations of the $[Cu_4I_4]$ and $[Cu_8I_8]$ cluster cores. In particular, bands at 90 and around 130 cm^{-1} can be attributed to Cu-I motion (wagging and stretching), in accordance with previous studies.[72–74] For the dimers (**C-StyD** and **C-EthylD**), the band at 90 cm^{-1} implies additionally the Cu-Cu stretching in the $[Cu_2I_2]$ connection between the two $[Cu_4I_4]$ units. The band around 130 cm^{-1} is slightly shifted for the two monomers with values of 127 and 133 cm^{-1} for **C-EthylM** and **C-StyM**, respectively. A broadening of these two bands is also detected for the dimers compared to the monomers, which can be explained by additional Cu-Cu and Cu-I vibrational modes corresponding to the $[Cu_2I_2]$ connection in the dimers and to modifications of the vibrations specific to the $[Cu_4I_4]$ moiety. The shape of these two low-frequency bands seems to allow differentiation of the two geometries of the cluster core.

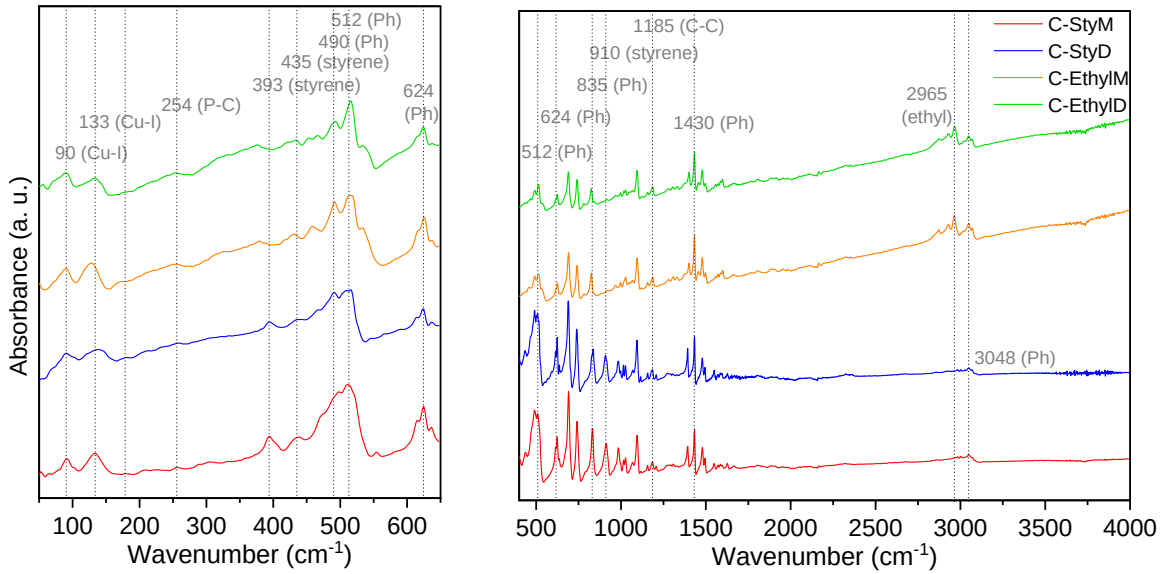

Figure 5. Far- and Mid-IR spectra of **C-Sty** and **C-Ethyl** clusters.

Raman spectra from 45 to 3500 cm^{-1} were recorded on single crystals and are presented in Figure 6. The four spectra present very similar signature with vibrations above 200 cm^{-1} coming from the ligands. The bands around 3050 cm^{-1} correspond to the C-H bonds stretching of the phenyl groups. Stretching of the ethyl group is observed at 2932 (CH_2) and 2975 cm^{-1} (CH_3) and bands attributed to the $CH=CH_2$ group are found at 1393, 1418 and 1628 cm^{-1} for the styrene derivatives. Below 200 cm^{-1}, an obvious similarity between the signature of the monomers (**C-StyM** and **C-EthylM**) and the dimers (**C-StyD** and **C-EthylD**) can be noticed with a broader shape for the former. Such broad feature have been already noticed for sulphur-based derivatives.[75] As in the IR spectra, in this low frequency region, vibrations of the $[Cu_4I_4]$ and $[Cu_8I_8]$ cluster cores take place. Five low frequencies bands at 67, 79, 96, 120 and 173 cm^{-1} are observed for **C-StyM** which are attributed to Cu-Cu and Cu-I stretching, rocking and breathing movements (Table S2-5). For **C-StyD**, the last four bands are also observed excepted the one at 67 cm^{-1}. This is similar for the ethyl derivatives with four bands at 72, 96, 120 and 177 cm^{-1} for **C-EthylM** and for **C-EthylD**, the 72 cm^{-1} band (Cu-I and Cu-Cu stretching) is missing and the 96 cm^{-1} one is less pronounced. Therefore, a distinct Raman signature characterizes the monomers and the dimers clusters.

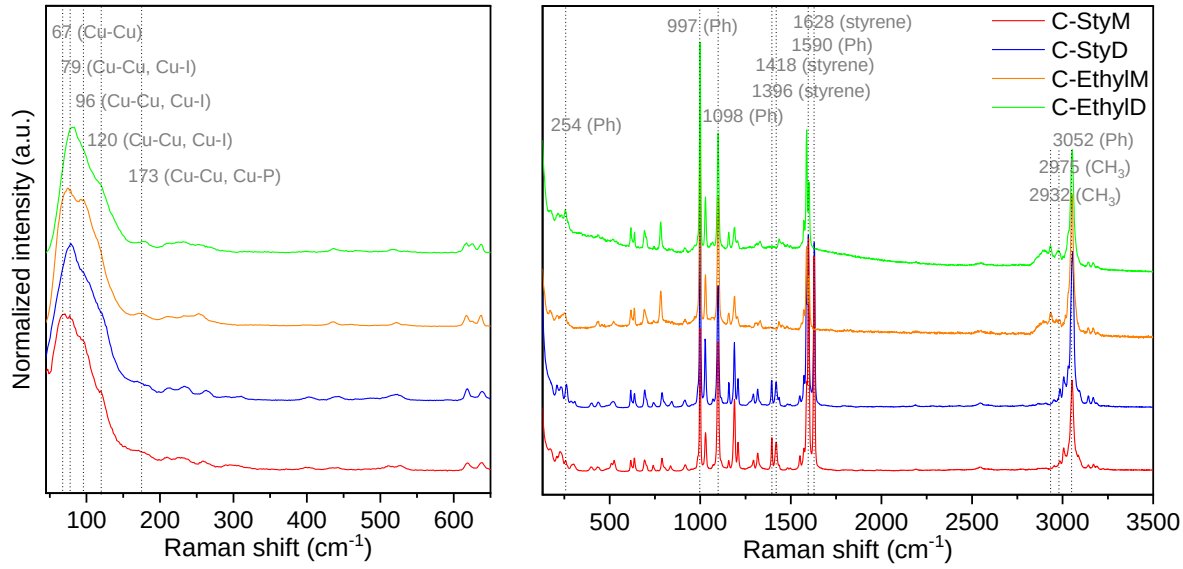

Figure 6. Raman spectra of **C-Sty** and **C-Ethyl** clusters.

Photophysical properties.

The clusters are white crystalline powders under ambient light. At room temperature, under classical UV excitation (365 nm UV lamp), no emission is observed for **C-StyM** and **C-StyD** with the naked eye whereas **C-EthylM** and **C-EthylD** present a bright yellow emission (Figure 7). While they present classical structural features for emitting copper iodide clusters, the non-luminescence of the styrene derivatives is surprising for such copper iodide clusters which usually display an intense emission such as the ethyl derivatives do. Excitation at lower energy (around 420 nm) allowed however detecting a weak green emission for **C-StyM** and **C-StyD** (Figure 8). The luminescence thermochromism of the **C-Ethyl** clusters is revealed when cooled in liquid nitrogen by displaying a contrasted emission color change from yellow to blue or whitish (Figure 7). When the samples are progressively warmed up to room temperature, the original emissions are recovered, indicating a completely reversible thermochromic luminescence phenomenon for **C-Ethyl** clusters.

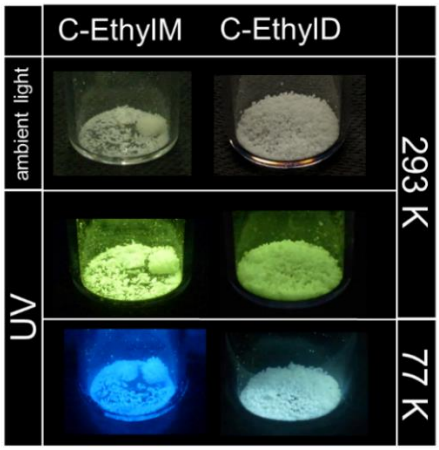

Figure 7. Photos of crystalline powders of **C-Ethyl** clusters, under visible light and under UV irradiation at 365 (UV lamp) at room temperature (295 K) and in liquid nitrogen (77 K).

Solid-state emission and excitation spectra were recorded from room temperature to 77 K and are reported in Figure 8 with data summarized in Table 2. Photoluminescence maps (emission 320-450 nm *vs* excitation 400-800 nm) recorded at 293 K are presented aside. The styrene derivatives have clearly an excitation range at lower energy compared with that of the ethyl ones. An emission of weak intensity centered at 575 nm is indeed observed for **C-StyM** and at 540 nm of **C-StyD**, under excitation at λ_{ex} = 430 and 415 nm, respectively. The Stokes shifts (difference between emission and excitation maxima) are 5860 and 5580 cm^{-1} for **C-StyM** and **C-StyD**, respectively. The emission band of **C-EthylM** and **C-EthylD**, are centered at 555 and 550 nm for an excitation at λ_{ex} = 360 nm and corresponding Stokes shifts are 9760 and 9600 cm^{-1}, respectively. The redshift in excitation of the styrene derivatives is in agreement with the recorded UV-Vis. absorption spectra with absorption at higher energy for the ethyl clusters (Figure S23). The absorption spectra also show that in the high-energy range (250-350 nm), all the four clusters absorb but in the case of the styrene derivatives this does not lead to the cluster's emission.

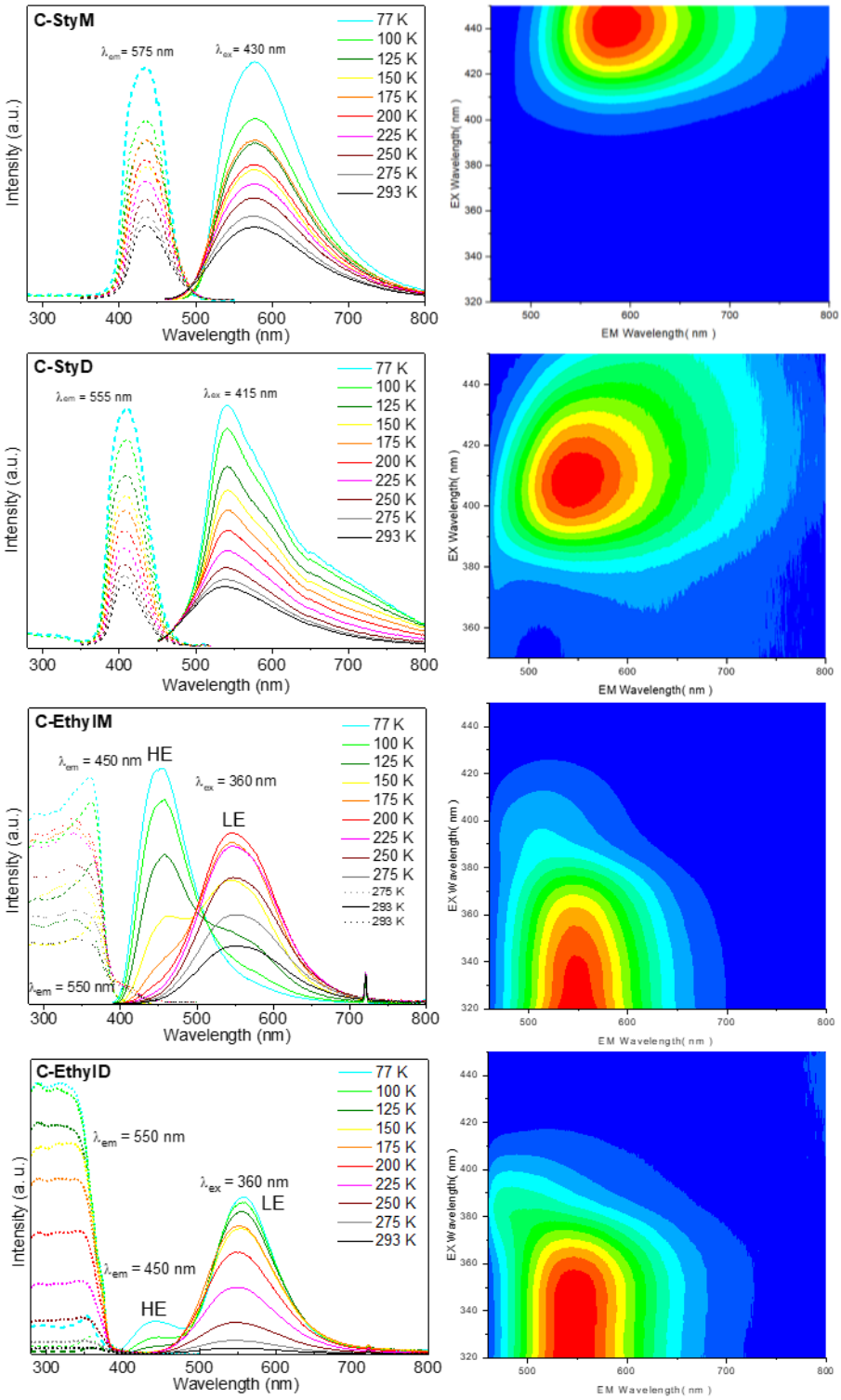

Figure 8. Solid-state luminescence spectra of the clusters. Left: emission *vs* excitation photoluminescence map recorded at 293 K. Right: temperature dependent emission in solid lines and excitation spectra in dashed (λ_{em} = 450 nm) or dotted lines (λ_{em} = 550 nm). For **C-Ethyl** clusters, small peaks at 720 nm are excitation artefact.

Upon decreasing the temperature, the intensity of the emission bands of **C-StyM** and **C-StyD** increase with no significant energy shift. Increasing radiative processes at low temperature is a well-known phenomenon. The shape of the excitation spectra are also unchanged with the temperature. In contrast,

C-EthylM and **C-EthylD** present an additional band at low temperature, and the relative intensity of the two bands varies with the temperature (λ_{ex} = 360 nm). At 77 K, the intense emission centered at 450 nm of **C-EthylM**, namely the HE (High Energy) band, agrees with the blue luminescence observed (Figure 7). For **C-EthylD**, this additional HE band centred at 440 nm is of lower intensity but induces the observed whitish emission. Similar behaviour was reported for the dimer $[Cu_8I_8(4\text{-dpda})_6]$ according to its close structural characteristics.[65] The progressive extinction of the HE band upon warming is accompanied by the emergence of the other one, namely LE (Low Energy), observed solely at room temperature, that is in agreement with the yellow light observed for **C-Ethyl**. Only small shift of the LE emission maxima is observed with the temperature (164 and 228 cm^{-1} for **C-EthylM** and **C-EthylD**, respectively). The excitation profiles of the two emission bands of both clusters are relatively similar. As expected, the Stokes shift of the HE bands is smaller than that of the LE ones with values of 5560 and 5050 cm^{-1}, for **C-EthylM** and **C-EthylD**, respectively. Classical luminescence thermochromism of cubane $[Cu_4I_4L_4]$ clusters is thus displayed by the ethyl derivatives in opposite to the styrene analogues.

Emission lifetimes recorded at room temperature for the styrene clusters indicate biexponential decays with τ_1 = 0.05, τ_2 = 0.48 µs for **C-StyM** and τ_1 = 0.08, τ_2 = 0.62 µs for **C-StyD** (Table 2 and Figure S22). **C-EthylM** presents a monoexponential decay with τ = 1.07 µs. The decay of **C-EthylD** is better fitted by a biexponential model with τ_1 = 0.08, τ_2 = 0.46 µs. Whereas monoexponential decay are common for cubane clusters, biexponential ones have been occasionally reported[42,59] but the exact origin has not yet been elucidated. The absolute internal photoluminescence quantum yields (PLQY) determined at room temperature are of 19 and 2 % for **C-EthylM** and **C-EthylD** and 2 and 0.5 % for **C-StyM** and **C-StyD**, respectively (Table 2). The monomers thus present higher PLQY compared with the dimers for the same ligand. The highest PLQY value of **C-EthylM** is also in accordance to its longer and single component lifetime indicative of a more effective radiative process in this case, less subject to surrounding disturbances.

Table 2. Experimental photoluminescence data of the clusters at different temperature. Lifetimes (τ) with pre-exponential factor in % and quantum yields (QY) were measured at 293 K. The values in brackets are the excitation or the emission wavelength.

	λ_{max} (nm) [λ_{ex} (nm)]		τ (µs) [λ_{ex} (nm)]	PLQY (%) [λ_{ex} (nm)]
	293 K	**77 K**		
C-StyM	575 [430]	576 [430]	0.05 (72%) / 0.48 (28%) [400]	2 [430]
C-StyD	540 [415]	541 [415]	0.08 (73%) / 0.62 (27%) [400]	0.5 [415]
C-EthylM	555 [360]	550 [360] (LE) 450 [360] (HE)	1.07 [267]	19 [360]
C-EthylD	550 [360]	557 [360] (LE) 440 [360] (HE)	0.08 (57%) / 0.46 (43%) [267]	2 [360]

DFT calculations.

DFT calculations were conducted for the four clusters using Gaussian software[76] (details in SI). The SCXRD experimental geometries, when available, were used as initial point for the structural optimization of the clusters structure. The ground state (S_0) of the clusters and the lowest triplet states (T_1 for the styrene derivatives, and T_1 and T_2 for the ethyl ones) were simulated (details in SI). Selected geometrical parameters of the different optimized states are given in Table 3 and their related structures are depicted in Figure S12-15. The computed bond lengths at the ground state (S_0) are in relative good

agreement with the experimental ones, although the Cu-Cu, Cu-I and Cu-P bond lengths are slightly overestimated due to the used basis set, as already reported (Table 3).[74]

Table 3. Geometrical parameters (mean values) of the optimized DFT structures at the S_0, and T_1 and T_2 states along with the experimental (mean) structural data (in squared brackets).

	C-StyM		**C-StyD**		**C-EthylM**			**C-EthylD**		
	S_0	**T_1**	**S_0**	**T_1**	**S_0**	**T_1** (HE)	**T_2** (LE)	**S_0**	**T_1** (HE)	**T_2** (LE)
Cu-Cu (Å)	2.998 [2.941(2)]	3.001	2.951 [2.947(1)]	2.948	3.005	2.996	2.758	2.960 [2.951(2)]	2.948	2.816
Cu-I (Å)	2.719 [2.686(2)]	2.719	2.719 [2.678(1)]	2.719	2.720	2.716	2.874	2.720 [2.683(2)]	2.709	2.766
Cu-P (Å)	2.347 [2.260(4)]	2.347	2.342 [2.251(1)]	2.342	2.347	2.348	2.362	2.342 [2.250(3)]	2.340	2.347

The electronic structures of the ground states were investigated and the Kohn-Sham orbital diagrams are reported in Figure 9. The HOMO-LUMO (highest occupied molecular orbital-lowest unoccupied molecular orbital) gaps are all found around 4 eV, indicating a strong thermodynamic stability. It should be noted that the gap increases slightly when transitioning from monomers to dimers, indicating enhanced stability. However, a significantly greater stabilization is simulated upon ligand substitution. The clusters with ethyl moieties are much more stable compared to the one with styrene group, as the latter have much lower energy levels for its LUMOs (Figure 9). This is likely a result of the interaction between the π* orbitals of the C=C moieties and the phenyl groups. This interaction lowers the energy levels of the first LUMOs, thereby slightly decreasing the overall stability.

The HOMO of the four clusters are all mainly based on Cu(*d*) and I(*p*) orbitals with significant contributions (between 35 and 40 %, respectively). The LUMOs are mostly composed of the ligands orbitals with a contribution of the π* orbitals of the phenyl groups around 90 %. We now shift our focus to the electronic properties of the Cu_4-based monomers, specifically **C-StyM** and **C-EthylM**. As anticipated for such clusters, the first 24 lowest orbitals (LUMO to LUMO+23) correspond to the π* orbitals, while the LUMO+24 is centered on the Cu atoms (~ 80 %) in a bonding combination. The range of these π* orbitals is 1.49 eV for **C-StyM** and 0.92 eV for **C-EthylM** (ΔE_2 in Figure S20). While **C-EthylM** presents a typical value for cubane clusters,[58,74] the larger energy range observed for **C-StyM** can be attributed to the styrene group. Indeed, the LUMO to LUMO+3 of **C-StyM** comprise the π* orbitals of styrene group and a significant gap of 0.36 eV (ΔE_3 in Figure S20) is found between the LUMO+3 and LUMO+4. The dispersion of the π* orbitals in **C-StyM** makes difficult the access to the Cu-centered orbital (e.g., LUMO+24), which is often responsible for an emission band for this family of clusters. In contrast, the π* orbitals block is approximately 40 % smaller for **C-EthylM**, enabling electrons to readily transit to the Cu-centered orbital and initiate emission. Note furthermore, the LUMO+23-LUMO+24 gaps all present similar values (ΔE_4 = 0.26 and 0.27 eV, in Figure S20). A similar trend is observed in the simulated electronic structures of the dimers, **C-StyD** and **C-EthylD** (ΔE_2 = 1.42 *vs*.0.87 eV, respectively). For **C-StyD**, the main contribution of the styrene orbitals are in the LUMO to LUMO+5 gathering and a 0.22 eV gap is observed between LUMO+5 and LUMO+6 (ΔE_3 in Figure S20). In both **C-StyD** and **C-EthylD**, the Cu bonding orbital (Cu ~ 70 %) corresponds to LUMO+37 and is slightly lower in energy compared to the monomer orbitals. This is because in the dimers, both Cu_4 entities are in an intra-bonding combination, along with a non-negligible inter-Cu_4 antibonding combination (in Cu_2I_2 connection). As a result, this orbital experiences a slight stabilization of approximately 0.05 eV in both cases. It is worth noting that intercalated within the block of the π* orbitals, are orbitals having significant Cu(s) contribution (~20 %) which are localized on the Cu_2I_2

connection between the two Cu_4 moieties. As already reported in previous investigations,[58,74] the electronic transitions of lowest energy calculated by TD-DFT (Time Dependent-DFT) are characterized as mixed halogen- and metal-to-ligand charge transfers, namely ^{1}(X+M)LCT. For the styrene derivatives, the π* orbitals of the styrene group are also implied whereas for the ethyl derivatives, only the π* phenyl orbitals are involved. Furthermore, it is worth mentioning that the stabilization of the π* orbitals in the styrene group leads to transitions occurring at lower energy levels (~3.40 eV, ~365 nm) compared to the transitions in the ethyl compounds (~3.82 eV, ~325 nm, Table S6). This is in accordance with the redshift observed in the absorption spectra of the styrene derivatives compared with the ethyl ones (Figure S23).

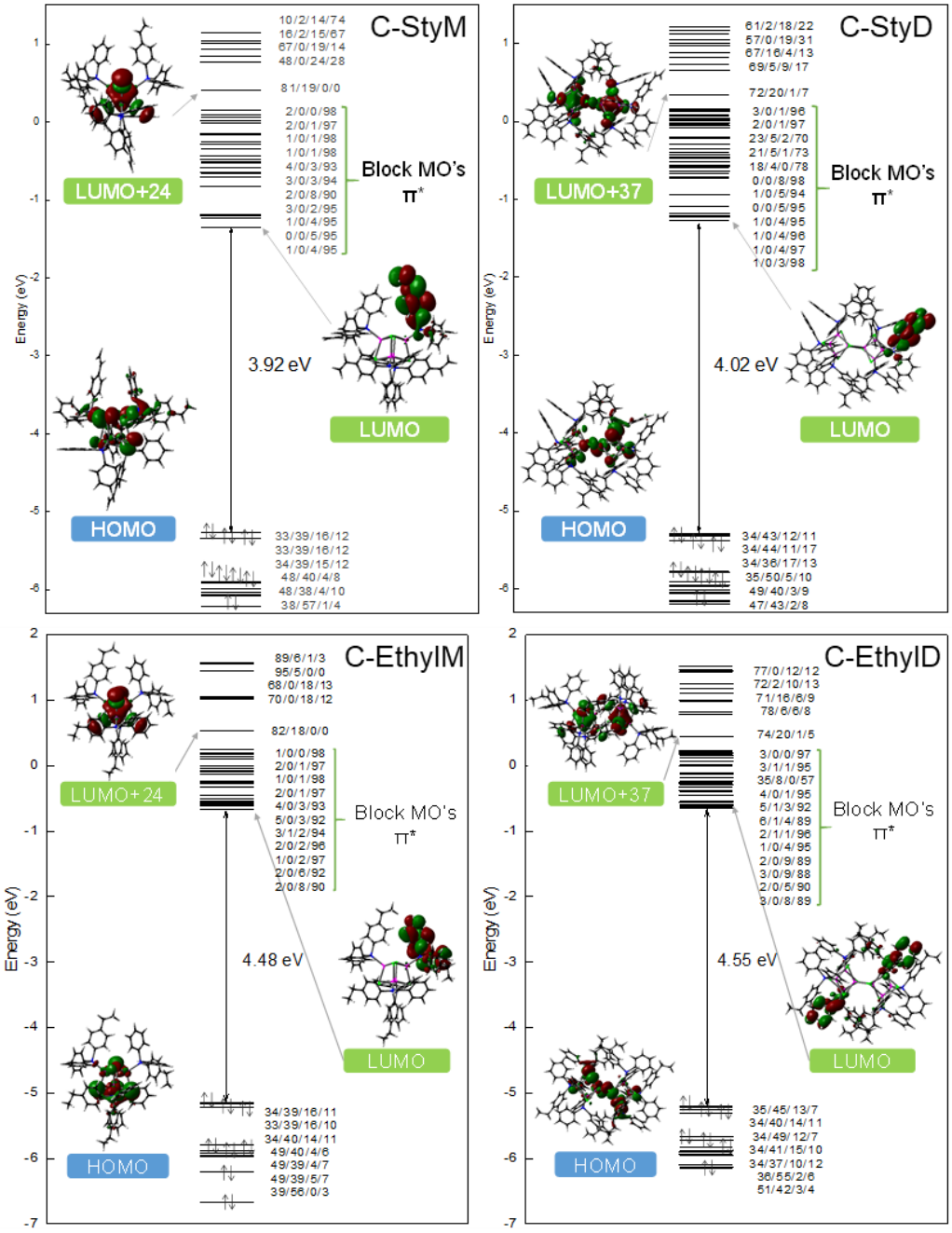

Figure 9. Kohn-Sham orbital diagrams of the clusters at the ground state (S_0). Orbital compositions correspond to Cu/I/P/Ph.

We now focus the discussion on the triplet excited states and the related luminescence properties. One triplet excited state was computed for the styrene derivatives (T_1) which correspond to the electron promotion from the HOMO (Cu and I) into one (or a combination) of the π* orbitals. The corresponding transition is thus of ^{3}(X+M)LCT character. The calculated electronic (not vibronic) vertical emission wavelengths are around 645 nm and slightly overestimate the experimental ones by 0.23 and 0.37 eV (575 and 540 nm), for **C-StyM** and **C-StyD**, respectively. Similar Cu-Cu, Cu-P and Cu-I distances of the triplet structures suggest the same calculated triplet state for the two clusters (Table 3). A possible explanation for the absence of a second triplet state emission, often referred to a ^{3}CC transition (Cluster Centered defined below), can be attributed to the lower energy levels of the π* orbitals formed by the $CH=CH_2$ of the styrene groups compared to the (pure) phenyl orbitals in the ethyl derivatives. As already mentioned, an initial π* block emerges (Figure S20), potentially capturing the electron and preventing its promotion to the bonding Cu_4 orbital (LUMO+24 for M or +37 for D) that would trigger the second emission. Furthermore, the low energy of these LUMOs are also responsible for the observed redshift of the emission compared with the ^{3}(X+M)LCT of other copper iodide clusters (HE band).

Two triplet states (T_1 and T_2) were computed for **C-Ethyl** cluster**s**, potentially explaining the observed two emission bands (HE and LE). As for the styrene derivatives, the T_1 excited state is of ^{3}(X+M)LCT character. The T_2 excited state of lower energy was obtained by promoting an electron from the HOMO (localized on Cu and I atoms) into the Cu-Cu bonding orbital, the LUMO+24 (**C-EthylM**) or LUMO+37 (**C-EthylD**). The corresponding transition is thus of mixed XMCT and MM character and is commonly referred to ^{3}CC. According to the bonding fashion combination in the Cu_4 cluster core for these orbitals, a significant Cu-Cu bond-length shortening is expected. This fact is fully confirmed for both **C-EthylM** and **C-EthylD** (Table 3 and Figure S21). The T_2 structure shows one iodine atom far from the copper atom (4.15 Å), that has been already reported.[58] The calculated emission wavelengths for **C-EthylM** of 523 and 656 nm for T_1 and T_2 respectively, are in acceptable agreement with the experimental ones of 450 and 555 nm for the HE and LE bands, respectively (Table S6). For the **C-EthylD**, the HE band is well reproduced by our simulations (459 nm *vs*. 440 nm) but the LE is still overestimating the experimental one (665 nm *vs.* 550 nm). The observed luminescence thermochromism characterized by a change of the relative intensity of the two emission bands can be thus explained by the thermal equilibrium of the corresponding two excited states, as reported for copper iodide clusters.[59,77,74] At low temperature, T_1 is preferentially populated (HE band) and upon increasing the temperature, it starts to be drained in detriment of the T_2 state (LE band). It should be emphasized that the LUMO+37 of **C-EthylD** demonstrates a strong bonding character within each Cu_4 moiety and a slight antibonding character in between (Cu_2I_2 connection). In order to further characterize the excited state behaviors, analyses of the spin densities were conducted (Figure 10). According to our simulations, the excited state density for the LE band of **C-EthylD** is predominantly localized on one Cu_4 moiety instead of being delocalized across the two (Figure 10). As a result, the excited state structure for this ^{3}CC transition exhibits a lengthening of the Cu-Cu contact in the Cu_2I_2 connection by ~0.15 Å (~4 %). The spin densities also fully assess the fact that for the ^{3}(X+M)LCT transition (HE band), the π* orbitals are occupied. In contrast, the spin density is clearly localized on a Cu_4 cluster core for the second observed emission (LE band), and therefore fully confirm the ^{3}CC character of this excited state (Figure 10).

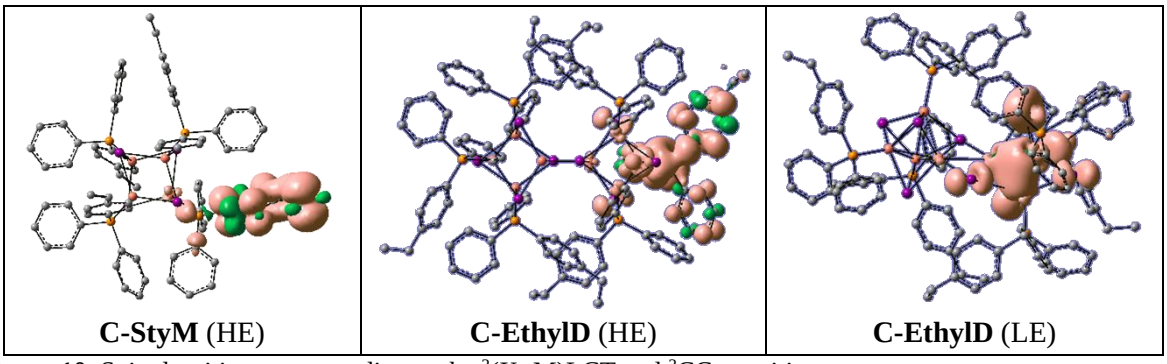

Figure 10. Spin densities corresponding to the ^{3}(X+M)LCT and ^{3}CC transitions.

Additionally, electron localization function (ELF), depicted around three Cu atoms of a Cu_4 core for all the clusters (Figure 11) were analyzed in their various simulated excited states (^{3}(X+M)LCT and ^{3}CC). For the ^{3}(X+M)CT transition, the ELF value at the center of the Cu_3 triangle is close to zero. Conversely, for the ^{3}CC one, a significant spin density is centered on the Cu_4 cluster core, the ELF value is around 0.5 at the center of the triangle (Figure 11). This indicates the presence of shared electrons, a non-negligible bonding character associated to the shortening of the Cu-Cu bond lengths (Figure S21), and is associated with a jellium-like electron distribution. These results confirm the different origin of the two HE and LE emission bands, ^{3}(X+M)CT and ^{3}CC, respectively, and their respective attribution.

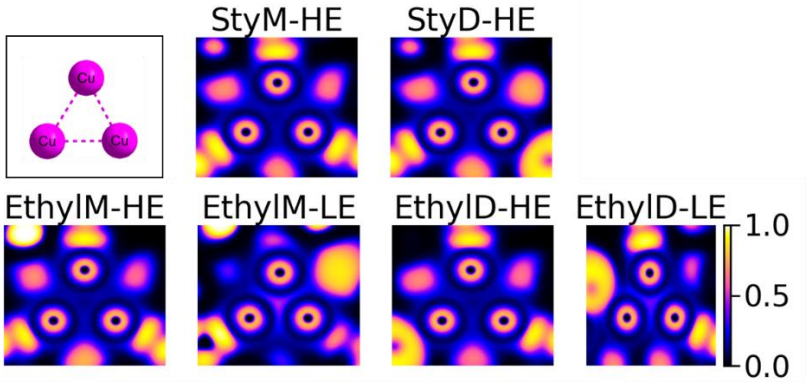

Figure 11. Electron localization function (ELF) for the ^{3}(X+M)LCT (HE) and ^{3}CC (LE) transitions of the four clusters.

Conclusion.

Two sets of molecular copper iodide clusters based on the cubane core were comparatively studied; monomers based on a single $[Cu_4I_4]$ motif and $[Cu_8I_8]$ dimers which present a rare geometry resulting from the connection of two tetranuclear monomers. Monomers and dimers were both obtained from the same reacting media suggesting an equilibrium in solution and their similar energies of formation, that are confirmed by the DFT calculations. The competitive formation of one cluster over another illustrates the versatility of copper(I) coordination ability. The investigation of two different phenylphosphine ligands permit to evaluate the effect of different substituent on the photophysical properties. Whereas the ethyl substituent leads to classical photoluminescence behavior for the corresponding clusters, the alkene chain on the styrene moieties has a great impact even though the structural characterizations indicate similar structures. No significant distortion of the cubane cluster cores upon dimerization is neither observed with a Cu_2I_2 connection presenting classical geometric feature for copper iodides.

While the structural differences are minor on the [Cu_4I_4] motif, the monomer and dimers can be easily distinguished from their specific signatures in solid-state ^{63}Cu NMR, Raman and IR analyses. Indeed, the Cu_2I_2 connection in the dimers significantly enlarge and modify the shape of the ^{63}Cu NMR spectra. Solid-state NMR technique is thus particularly powerful to distinguish the different cluster core geometries. By combining experimental IR and Raman spectroscopies with DFT calculations, the vibrational signature of these clusters could have been interpreted. Future work will be conducted to improve accuracy of the IR and Raman spectra simulation by using anharmonic approximation that is quite challenging for such large systems.

The monomer and the dimer of a same ligand present relatively similar photophysical properties. With the ethyl ligands, luminescence thermochromism is observed with two emission bands namely ^{3}(X+M)LCT and ^{3}CC, whose respective intensity varies with the temperature. This behaviour, quite classical for copper iodide clusters, contrasts with the styrene derivatives which display an original photoluminescence with a single emission band excited at lower energy. The DFT calculations permit to ascribe this unclassical emission band to a ^{3}(X+M)LCT transition which is importantly modified by the presence of additional vacant orbitals based on the styrene group. In particular, its shift to lower energy can be attributed to the lower energy of these styrene-based orbitals by delocalization over the double bond. The presence of these unoccupied orbitals has another consequence: the lack of a second emission band for the styrene derivatives. Indeed, their lower energy compared with orbitals based solely on phenyl groups, creates a gap within the ligand-based block of orbitals that renders less favorable transitions of higher energy such as the ^{3}CC one. The styrene group acts somehow as a quencher of luminescence.

This study demonstrates that original copper iodide complexes of high nuclearity are accessible thanks to the structural flexibility in this family of compounds, in adequate experimental conditions. In the studied cases, the nuclearity of copper iodide clusters has eventually less influence on the photophysical properties than the nature of the ligand. By a neat choice of the electronic properties of the ligands, it may be possible to control and tune the photophysical properties of the corresponding clusters. This is a relevant perspective for developing materials for specific lighting applications.

Supporting Information.

Details of synthetic procedures, experimental details, characterizations data and additional figures (crystal structures, IR, Raman, calculated molecular orbitals). This information is available free of charge at http://pubs.acs.org.

Acknowledgments.

The 'Région Pays de la Loire' and 'Agence de l'Innovation de Défense' are thanked for the Ph.D. fellowship of R. Utrera-Melero. C. Martineau-Corcos is grateful for financial support from the Institut Universitaire de France (IUF). Financial support from the IR INFRANALYTICS FR2054 for conducting the research is gratefully acknowledged. The CCIPL (Centre de Calculs Intensifs des Pays de Loire) is acknowledged for computational resources.

References.

(1) Wenger, O. S. Photoactive Complexes with Earth-Abundant Metals. *J. Am. Chem. Soc.* **2018**, *140* (42), 13522–13533. https://doi.org/10.1021/jacs.8b08822.
(2) Hamze, R.; Peltier, J. L.; Sylvinson, D.; Jung, M.; Cardenas, J.; Haiges, R.; Soleilhavoup, M.; Jazzar, R.; Djurovich, P. I.; Bertrand, G.; Thompson, M. E. Eliminating Nonradiative Decay in Cu(I) Emitters: >99% Quantum Efficiency and Microsecond Lifetime. *Science* **2019**, *363* (6427), 601–606. https://doi.org/10.1126/science.aav2865.
(3) Han, L.; Sun, B.; Guo, C.; Peng, G.; Chen, H.; Yang, Z.; Li, N.; Ci, Z.; Jin, Z. Photophysics in Zero-Dimensional Potassium-Doped Cesium Copper Chloride Cs3Cu2Cl5 Nanosheets and Its Application for High-Performance Flexible X-Ray Detection. *Adv. Opt. Mater.* **2022**, *10* (6), 2102453. https://doi.org/10.1002/adom.202102453.
(4) Su, B.; Jin, J.; Han, K.; Xia, Z. Ceramic Wafer Scintillation Screen by Utilizing Near-Unity Blue-Emitting Lead-Free Metal Halide (C8H20N)2Cu2Br4. *Advanced Functional Materials* **2023**, *33* (5), 2210735. https://doi.org/10.1002/adfm.202210735.
(5) Li, S.; Xu, J.; Li, Z.; Zeng, Z.; Li, W.; Cui, M.; Qin, C.; Du, Y. One-Dimensional Lead-Free Halide with Near-Unity Greenish-Yellow Light Emission. *Chem. Mater.* **2020**, *32* (15), 6525–6531. https://doi.org/10.1021/acs.chemmater.0c01794.
(6) Beaudelot, J.; Oger, S.; Peruško, S.; Phan, T.-A.; Teunens, T.; Moucheron, C.; Evano, G. Photoactive Copper Complexes: Properties and Applications. *Chem. Rev.* **2022**, *122* (22), 16365–16609. https://doi.org/10.1021/acs.chemrev.2c00033.
(7) Zink, D. M.; Volz, D.; Baumann, T.; Mydlak, M.; Flu, H.; Friedrichs, J.; Nieger, M.; Bras, S. Heteroleptic, Dinuclear Copper(I) Complexes for Application in Organic Light-Emitting Diodes. *Chem. Mater.* **2013**, *25*, 4471−4486. https://doi.org/10.1021/cm4018375.
(8) You, Z.; Li, H.; Zhang, L.; Yu, B.; Zhang, J.; Wu, X. A Host Material for Deep-Blue Electrophosphorescence Based on a Cuprous Metal–Organic Framework. *J. Phys. Chem. C* **2017**, *121* (41), 23072–23079. https://doi.org/10.1021/acs.jpcc.7b07627.
(9) Liu, Y.; Yiu, S.-C.; Ho, C.-L.; Wong, W.-Y. Recent Advances in Copper Complexes for Electrical/Light Energy Conversion. *Coord. Chem. Rev.* **2018**, *375*, 514–557. https://doi.org/10.1016/j.ccr.2018.05.010.
(10) Olaru, M.; Rychagova, E.; Ketkov, S.; Shynkarenko, Y.; Yakunin, S.; Kovalenko, M. V.; Yablonskiy, A.; Andreev, B.; Kleemiss, F.; Beckmann, J.; Vogt, M. A Small Cationic Organo–Copper Cluster as Thermally Robust Highly Photo- and Electroluminescent Material. *J. Am. Chem. Soc.* **2020**, *142* (1), 373–381. https://doi.org/10.1021/jacs.9b10829.
(11) Takeda, H.; Kobayashi, A.; Tsuge, K. Recent Developments of Photoactive Cu(I) and Ag(I) Complexes with Diphosphine and Related Ligands. *Coord. Chem. Rev.* **2022**, *470*, 214700. https://doi.org/10.1016/j.ccr.2022.214700.
(12) Baghdasaryan, A.; Bürgi, T. Copper Nanoclusters: Designed Synthesis, Structural Diversity, and Multiplatform Applications. *Nanoscale* **2021**, *13* (13), 6283–6340. https://doi.org/10.1039/D0NR08489A.
(13) Yam, V. W.-W.; Au, V. K.-M.; Leung, S. Y.-L. Light-Emitting Self-Assembled Materials Based on d^8 and d^{10} Transition Metal Complexes. *Chem. Rev.* **2015**, *115* (15), 7589–7728. https://doi.org/10.1021/acs.chemrev.5b00074.
(14) Fang, Y.; Sojdak, C. A.; Dey, G.; Teat, S. J.; Li, M.; Cotlet, M.; Zhu, K.; Liu, W.; Wang, L.; ÓCarroll, D. M.; Li, J. Highly Efficient and Very Robust Blue-Excitable Yellow Phosphors Built on Multiple-Stranded One-Dimensional Inorganic–Organic Hybrid Chains. *Chem. Sci.* **2019**, *10* (20), 5363–5372. https://doi.org/10.1039/C9SC00970A.
(15) Liu, W.; Zhou, Z.; Li, H.; Lv, Y.; Tong, H.; Zhu, J.; Ouyang, G. New Strategy for Optimizing the Properties of Copper Halide Organic-Inorganic Hybrid Lighting-Emitting Materials. *Chemistry – A European Journal* **2022**, *28* (71), e202202478. https://doi.org/10.1002/chem.202202478.
(16) Hei, X.; Li, J. All-in-One: A New Approach toward Robust and Solution-Processable Copper Halide Hybrid Semiconductors by Integrating Covalent, Coordinate and Ionic Bonds in Their Structures. *Chem. Sci.* **2021**, *12* (11), 3805–3817. https://doi.org/10.1039/D0SC06629J.
(17) Wang, S.; Morgan, E. E.; Panuganti, S.; Mao, L.; Vishnoi, P.; Wu, G.; Liu, Q.; Kanatzidis, M. G.; Schaller, R. D.; Seshadri, R. Ligand Control of Structural Diversity in Luminescent Hybrid Copper(I) Iodides. *Chem. Mater.* **2022**, *34* (7), 3206–3216. https://doi.org/10.1021/acs.chemmater.1c04408.
(18) Liu, G.-N.; Xu, R.-D.; Zhao, R.-Y.; Sun, Y.; Bo, Q.-B.; Duan, Z.-Y.; Li, Y.-H.; Wang, Y.-Y.; Wu, Q.; Li, C. Hybrid Copper Iodide Cluster-Based Pellet Sensor for Highly Selective Optical Detection of o-Nitrophenol and Tetracycline Hydrochloride in Aqueous Solution. *ACS Sustainable Chem. Eng.* **2019**, *7* (23), 18863–18873. https://doi.org/10.1021/acssuschemeng.9b03963.

(19) Artem'ev, A. V.; Davydova, M. P.; Hei, X.; Rakhmanova, M. I.; Samsonenko, D. G.; Bagryanskaya, I. Yu.; Brylev, K. A.; Fedin, V. P.; Chen, J.-S.; Cotlet, M.; Li, J. Family of Robust and Strongly Luminescent CuI-Based Hybrid Networks Made of Ionic and Dative Bonds. *Chem. Mater.* **2020**, *32* (24), 10708–10718. https://doi.org/10.1021/acs.chemmater.0c03984.
(20) Chen, C.-Y.; Lin, Y.-I.; Lai, P.-T.; Lin, H.-C.; Tan, G.-H.; Lin, H.-W.; Schaller, R. D. Self-Trapped and Free Exciton Dynamics in Vacuum-Deposited Cesium Copper Iodide Thin Films. *Adv. Opt. Mater.* **2022**, *10* (17), 2200005. https://doi.org/10.1002/adom.202200005.
(21) Lian, L.; Zheng, M.; Zhang, P.; Zheng, Z.; Du, K.; Lei, W.; Gao, J.; Niu, G.; Zhang, D.; Zhai, T.; Jin, S.; Tang, J.; Zhang, X.; Zhang, J. Photophysics in Cs3Cu2X5 (X = Cl, Br, or I): Highly Luminescent Self-Trapped Excitons from Local Structure Symmetrization. *Chem. Mater.* **2020**, *32* (8), 3462–3468. https://doi.org/10.1021/acs.chemmater.9b05321.
(22) Li, Y.; Zhou, Z.; Sheong, F. K.; Xing, Z.; Wong, K. S.; Sung, H. H. Y.; Williams, I. D.; Halpert, J. E. Organic–Inorganic Hybrid Alkali Copper Iodides for Bright Emission across the Visible Spectrum. *Chem. Mater.* **2023**, *35* (3), 1318–1324. https://doi.org/10.1021/acs.chemmater.2c03353.
(23) Zhu, K.; Cheng, Z.; Rangan, S.; Cotlet, M.; Du, J.; Kasaei, L.; Teat, S. J.; Liu, W.; Chen, Y.; Feldman, L. C.; O'Carroll, D. M.; Li, J. A New Type of Hybrid Copper Iodide as Nontoxic and Ultrastable LED Emissive Layer Material. *ACS Energy Lett.* **2021**, *6* (7), 2565–2574. https://doi.org/10.1021/acsenergylett.1c00993.
(24) Schlachter, A.; Tanner, K.; Harvey, P. D. Copper Halide-Chalcogenoether and -Chalcogenone Networks: Chain and Cluster Motifs, Polymer Dimensionality and Photophysical Properties. *Coord. Chem. Rev.* **2021**, *448*, 214176. https://doi.org/10.1016/j.ccr.2021.214176.
(25) Su, B.; Jin, J.; Peng, Y.; Molokeev, M. S.; Yang, X.; Xia, Z. Zero-Dimensional Organic Copper(I) Iodide Hybrid with High Anti-Water Stability for Blue-Light-Excitable Solid-State Lighting. *Advanced Optical Materials* **2022**, *10* (12), 2102619. https://doi.org/10.1002/adom.202102619.
(26) Zheng, H.-W.; Yang, D.-D.; Liang, Q.-F.; Liu, Y.-P.; Shan, J.-H.; Liu, Q.-Q.; Tan, H.-W.; Chen, L.; Zheng, X.-J. A Diamond-like Cuprous Coordination Polymer Based on the [Cu8I6]2+ Cluster with Multistimuli-Responsive Luminescence and Iodine Adsorption Behavior. *J. Mater. Chem. C* **2022**, *10* (10), 3901–3907. https://doi.org/10.1039/D1TC05937H.
(27) Strelnik, I.; Shamsieva, A.; Akhmadgaleev, K.; Gerasimova, T.; Dayanova, I.; Kolesnikov, I.; Fayzullin, R.; Islamov, D.; Musina, E.; Karasik, A.; Sinyashin, O. Emission and Luminescent Vapochromism Control of Octahedral Cu4I4 Complexes by Conformationally Restricted P,N Ligands. *Chemistry – A European Journal* **2023**, *29* (10), e202202864. https://doi.org/10.1002/chem.202202864.
(28) Kobayashi, A.; Kato, M. Stimuli-Responsive Luminescent Copper(I) Complexes for Intelligent Emissive Devices. *Chem. Lett.* **2017**, *46* (2), 154–162. https://doi.org/10.1246/cl.160794.
(29) Cariati, E.; Lucenti, E.; Botta, C.; Giovanella, U.; Marinotto, D.; Righetto, S. Cu(I) Hybrid Inorganic–Organic Materials with Intriguing Stimuli Responsive and Optoelectronic Properties. *Coord. Chem. Rev.* **2016**, *306*, 566–614. https://doi.org/10.1016/j.ccr.2015.03.004.
(30) Wallesch, M.; Volz, D.; Zink, D. M.; Schepers, U.; Nieger, M.; Baumann, T.; Bräse, S. Bright Coppertunities: Multinuclear CuI Complexes with NP Ligands and Their Applications. *Chem. Eur. J.* **2014**, *20*, 6578–6590. https://doi.org/10.1002/chem.201402060.
(31) Song, K.-H.; Wang, J.-J.; Feng, L.-Z.; He, F.; Yin, Y.-C.; Yang, J.-N.; Song, Y.-H.; Zhang, Q.; Ru, X.-C.; Lan, Y.-F.; Zhang, G.; Yao, H.-B. Thermochromic Phosphors Based on One-Dimensional Ionic Copper-Iodine Chains Showing Solid-State Photoluminescence Efficiency Exceeding 99 %. *Angew. Chem. Int. Ed.* **2022**, *61* (38), e202208960. https://doi.org/10.1002/anie.202208960.
(32) Kim, T. H.; Shin, Y. W.; Jung, J. H.; Kim, J. S.; Kim, J. Crystal-to-Crystal Transformation between Three CuI Coordination Polymers and Structural Evidence for Luminescence Thermochromism. *Angew. Chem. Int. Ed.* **2008**, *47* (4), 685–688. https://doi.org/10.1002/anie.200704349.
(33) Fu, Z.; Lin, J.; Wang, L.; Li, C.; Yan, W.; Wu, T. Cuprous Iodide Pseudopolymorphs Based on Imidazole Ligand and Their Luminescence Thermochromism. *Cryst. Growth Des.* **2016**, *16* (4), 2322–2327. https://doi.org/10.1021/acs.cgd.6b00114.
(34) Zhan, S.-Z.; Li, M.; Ng, S. W.; Li, D. Luminescent Metal-Organic Frameworks (MOFs) as a Chemopalette: Tuning the Thermochromic Behavior of Dual-Emissive Phosphorescence by Adjusting the Supramolecular Microenvironments. *Chem. Eur. J.* **2013**, *19* (31), 10217–10225. https://doi.org/10.1002/chem.201204632.
(35) Yersin, H.; Czerwieniec, R.; Monkowius, U.; Ramazanov, R.; Valiev, R.; Shafikov, M. Z.; Kwok, W.-M.; Ma, C. Intersystem Crossing, Phosphorescence, and Spin-Orbit Coupling. Two Contrasting Cu(I)-TADF Dimers Investigated by Milli- to Micro-Second Phosphorescence, Femto-Second Fluorescence, and Theoretical Calculations. *Coord. Chem. Rev.* **2023**, *478*, 214975. https://doi.org/10.1016/j.ccr.2022.214975.

(36) Nitsch, J.; Lacemon, F.; Lorbach, A.; Eichhorn, A.; Cisnetti, F.; Steffen, A. Cuprophilic Interactions in Highly Luminescent Dicopper(Ⅰ)–NHC–Picolyl Complexes – Fast Phosphorescence or TADF? *Chem. Commun.* **2016**, *52* (14), 2932–2935. https://doi.org/10.1039/C5CC09659F.
(37) Perruchas, S. Molecular Copper Iodide Clusters: A Distinguishing Family of Mechanochromic Luminescent Compounds. *Dalton Trans.* **2021**, *50* (35), 12031–12044. https://doi.org/10.1039/D1DT01827B.
(38) Shan, X.-C.; Jiang, F.-L.; Zhang, H.; Qian, X.-Y.; Chen, L.; Wu, M.-Y.; AL-Thabaiti, S. A.; Hong, M.-C. A Solid AND Logic Stimuli-Responsive Material with Bright Nondestructive Performance Designed by Sensitive Cuprophilicity. *Chem. Commun.* **2013**, *49* (87), 10227–10229. https://doi.org/10.1039/c3cc43241f.
(39) Yao, J.-S.; Wang, J.-J.; Yang, J.-N.; Yao, H.-B. Modulation of Metal Halide Structural Units for Light Emission. *Acc. Chem. Res.* **2021**, *54* (2), 441–451. https://doi.org/10.1021/acs.accounts.0c00707.
(40) Peng, R.; Li, M.; Li, D. Copper(I) Halides: A Versatile Family in Coordination Chemistry and Crystal Engineering. *Coord. Chem. Rev.* **2010**, *254* (1–2), 1–18. https://doi.org/10.1016/j.ccr.2009.10.003.
(41) Ford, P. C.; Cariati, E.; Bourassa, J. Photoluminescence Properties of Multinuclear Copper(I) Compounds. *Chem. Rev.* **1999**, *99* (12), 3625–3648. https://doi.org/10.1021/cr960109i.
(42) Benito, Q.; Le Goff, X. F.; Maron, S.; Fargues, A.; Garcia, A.; Martineau, C.; Taulelle, F.; Kahlal, S.; Gacoin, T.; Boilot, J.-P.; Perruchas, S. Polymorphic Copper Iodide Clusters: Insights into the Mechanochromic Luminescence Properties. *J. Am. Chem. Soc.* **2014**, *136* (32), 11311–11320. https://doi.org/10.1021/ja500247b.
(43) Kitagawa, H.; Ozawa, Y.; Toriumi, K. Flexibility of Cubane-like Cu4I4 Framework: Temperature Dependence of Molecular Structure and Luminescence Thermochromism of [Cu4I4(PPh3)4] in Two Polymorphic Crystalline States. *Chem. Commun.* **2010**, *46* (34), 6302–6304. https://doi.org/10.1039/c0cc01434f.
(44) Li, S.-L.; Zhang, X.-M. Cu_3I_7 Trimer and Cu_4I_8 Tetramer Based Cuprous Iodide Polymorphs for Efficient Photocatalysis and Luminescent Sensing: Unveiling Possible Hierarchical Assembly Mechanism. *Inorg. Chem.* **2014**, *53* (16), 8376–8383. https://doi.org/10.1021/ic500822w.
(45) Churchill, M. R.; Kalra, K. L. Molecules with an M4X4 Core. I . Crystal and Molecular Structure of Tetrameric Triphenylphosphinecopper(1) Chloride, a "Cubane-Like" Molecule, Including the Location and Refinement of All Hydrogen Atoms. *Inorg. Chem.* **1974**, *13* (5), 1065–1071. https://doi.org/10.1021/ic50135a011.
(46) Zhao, C.-W.; Ma, J.-P.; Liu, Q.-K.; Wang, X.-R.; Liu, Y.; Yang, J.; Yang, J.-S.; Dong, Y.-B. An in Situ Self-Assembled Cu_4I_4–MOF-Based Mixed Matrix Membrane: A Highly Sensitive and Selective Naked-Eye Sensor for Gaseous HCl. *Chem. Commun.* **2016**, *52* (30), 5238–5241. https://doi.org/10.1039/C6CC00189K.
(47) Cho, S.; Jeon, Y.; Lee, S.; Kim, J.; Kim, T. H. Reversible Transformation between Cubane and Stairstep Cu_4I_4 Clusters Using Heat or Solvent Vapor. *Chem. Eur. J.* **2015**, *21* (4), 1439–1443. https://doi.org/10.1002/chem.201405800.
(48) Park, H.; Kwon, E.; Chiang, H.; Im, H.; Lee, K. Y.; Kim, J.; Kim, T. H. Reversible Crystal Transformations and Luminescence Vapochromism by Fast Guest Exchange in Cu(I) Coordination Polymers. *Inorg. Chem.* **2017**, *56* (14), 8287–8294. https://doi.org/10.1021/acs.inorgchem.7b00951.
(49) Killarney, J. P.; McKinnon, M.; Murphy, C.; Henline, K. M.; Wang, C.; Pike, R. D.; Patterson, H. H. Amine- and Sulfide-Sensing Copper(I) Iodide Films. *Inorg. Chem. Com.* **2014**, *40*, 18–21. https://doi.org/10.1016/j.inoche.2013.11.022.
(50) Tran, D.; Bourassa, J. L.; Ford, P. C. Pressure-Induced Luminescence Rigidochromism in the Photophysics of the Cuprous Iodide Cluster Cu4I4py4. *Inorg. Chem.* **1997**, *36* (3), 439–442. https://doi.org/10.1021/ic960959g.
(51) Roppolo, I.; Celasco, E.; Sangermano, M.; Garcia, A.; Gacoin, T.; Boilot, J.-P.; Perruchas, S. Luminescence Variation by Rigidity Control of Acrylic Composite Materials. *J. Mater. Chem. C* **2013**, *1* (36), 5725. https://doi.org/10.1039/c3tc30407h.
(52) Xie, M.; Han, C.; Liang, Q.; Zhang, J.; Xie, G.; Xu, H. Highly Efficient Sky Blue Electroluminescence from Ligand-Activated Copper Iodide Clusters: Overcoming the Limitations of Cluster Light-Emitting Diodes. *Sci. Adv.* **2019**, *5* (6), eaav9857. https://doi.org/10.1126/sciadv.aav9857.
(53) Fang, Y.; Liu, W.; Teat, S. J.; Dey, G.; Shen, Z.; An, L.; Yu, D.; Wang, L.; O'Carroll, D. M.; Li, J. A Systematic Approach to Achieving High Performance Hybrid Lighting Phosphors with Excellent Thermal- and Photostability. *Adv. Funct. Mater.* **2017**, *27* (3), 1603444. https://doi.org/10.1002/adfm.201603444.
(54) Zhang, N.; Hu, H.; Qu, L.; Huo, R.; Zhang, J.; Duan, C.; Meng, Y.; Han, C.; Xu, H. Overcoming Efficiency Limitation of Cluster Light-Emitting Diodes with Asymmetrically Functionalized Biphosphine Cu4I4 Cubes. *J. Am. Chem. Soc.* **2022**, *144* (14), 6551–6557. https://doi.org/10.1021/jacs.2c01588.
(55) Xie, M.; Han, C.; Zhang, J.; Xie, G.; Xu, H. White Electroluminescent Phosphine-Chelated Copper Iodide Nanoclusters. *Chem. Mater.* **2017**, *29* (16), 6606–6610. https://doi.org/10.1021/acs.chemmater.7b01443.

(56) Liu, X.; Li, R.; Xu, X.; Jiang, Y.; Zhu, W.; Yao, Y.; Li, F.; Tao, X.; Liu, S.; Huang, W.; Zhao, Q. Lanthanide(III)-Cu4I4 Organic Framework Scintillators Sensitized by Cluster-Based Antenna for High-Resolution X-Ray Imaging. *Advanced Materials* **2023**, *35* (8), 2206741. https://doi.org/10.1002/adma.202206741.
(57) Miao, H.; Pan, X.; Li, M.; Zhaxi, W.; Wu, J.; Huang, Z.; Liu, L.; Ma, X.; Jiang, S.; Huang, W.; Zhang, Q.; Wu, D. A Copper Iodide Cluster-Based Coordination Polymer as an Unconventional Zero-Thermal-Quenching Phosphor. *Inorg. Chem.* **2022**, *61* (46), 18779–18788. https://doi.org/10.1021/acs.inorgchem.2c03322.
(58) Perruchas, S.; Tard, C.; Le Goff, X. F.; Fargues, A.; Garcia, A.; Kahlal, S.; Saillard, J.-Y.; Gacoin, T.; Boilot, J.-P. Thermochromic Luminescence of Copper Iodide Clusters: The Case of Phosphine Ligands. *Inorg. Chem.* **2011**, *50* (21), 10682–10692. https://doi.org/10.1021/ic201128a.
(59) Huitorel, B.; El Moll, H.; Utrera-Melero, R.; Cordier, M.; Fargues, A.; Garcia, A.; Massuyeau, F.; Martineau-Corcos, C.; Fayon, F.; Rakhmatullin, A.; Kahlal, S.; Saillard, J.-Y.; Gacoin, T.; Perruchas, S. Evaluation of Ligands Effect on the Photophysical Properties of Copper Iodide Clusters. *Inorg. Chem.* **2018**, *57* (8), 4328–4339. https://doi.org/10.1021/acs.inorgchem.7b03160.
(60) Bondi, A. Van Der Waals Volumes and Radii. *J. Phys. Chem.* **1964**, *68* (3), 441–451. https://doi.org/10.1021/j100785a001.
(61) Hou, Q.; Yu, J.-H.; Xu, J.-N.; Yang, Q.-F.; Xu, J.-Q. A New 3-D Two-Fold Interpenetrated Framework with Sqp Net Based on Cu6I6 and Cu8I8 Cluster Nodes. *CrystEngComm* **2009**, *11* (11), 2452. https://doi.org/10.1039/b902936m.
(62) Bi, M.; Li, G.; Hua, J.; Liu, Y.; Liu, X.; Hu, Y.; Shi, Z.; Feng, S. Two Isomers with FSC Topology Constructed from $Cu_6I_6(DABCO)_4$ and $Cu_8I_8(DABCO)_6$ Building Blocks. *Crystal Growth & Design* **2007**, *7* (10), 2066–2070. https://doi.org/10.1021/cg0700824.
(63) Bonnot, A.; Juvenal, F.; Lapprand, A.; Fortin, D.; Knorr, M.; Harvey, P. D. Can a Highly FLexible Copper(I) Cluster-Containing 1D and 2D Coordination Polymers Exhibit MOF-like Properties? *Dalton Trans.* **2016**, No. 45, 11413–11421.
(64) Knorr, M.; Bonnot, A.; Lapprand, A.; Khatyr, A.; Strohmann, C.; Kubicki, M. M.; Rousselin, Y.; Harvey, P. D. Reactivity of CuI and CuBr toward Dialkyl Sulfides RSR: From Discrete Molecular $Cu_4I_4S_4$ and $Cu_8I_8S_6$ Clusters to Luminescent Copper(I) Coordination Polymers. *Inorg. Chem.* **2015**, *54* (8), 4076–4093. https://doi.org/10.1021/acs.inorgchem.5b00327.
(65) Shan, X.-C.; Zhang, H.-B.; Chen, L.; Wu, M.-Y.; Jiang, F.-L.; Hong, M.-C. Multistimuli-Responsive Luminescent Material Reversible Switching Colors via Temperature and Mechanical Force. *Cryst. Growth Des.* **2013**, *13*, 377–1381.
(66) Tang, J. A.; Ellis, B. D.; Warren, T. H.; Hanna, J. V.; Macdonald, C. L. B.; Schurko, R. W. Solid-State ^{63}Cu and ^{65}Cu NMR Spectroscopy of Inorganic and Organometallic Copper(I) Complexes. *J. Am. Chem. Soc.* **2007**, *129* (43), 13049–13065. https://doi.org/10.1021/ja073238x.
(67) Huitorel, B.; Utrera-Melero, R.; Massuyeau, F.; Mevelec, J.-Y.; Baptiste, B.; Polian, A.; Gacoin, T.; Martineau-Corcos, C.; Perruchas, S. Luminescence Mechanochromism of Copper Iodide Clusters: A Rational Investigation. *Dalton Trans.* **2019**, *48* (22), 7899–7909. https://doi.org/10.1039/C9DT01161G.
(68) Benito, Q.; Le Goff, X. F.; Nocton, G.; Fargues, A.; Garcia, A.; Berhault, A.; Kahlal, S.; Saillard, J.-Y.; Martineau, C.; Trébosc, J.; Gacoin, T.; Boilot, J.-P.; Perruchas, S. Geometry Flexibility of Copper Iodide Clusters: Variability in Luminescence Thermochromism. *Inorg. Chem.* **2015**, *54* (9), 4483–4494. https://doi.org/10.1021/acs.inorgchem.5b00321.
(69) Harris, R. K.; Olivieri, A. C. Quadrupolar Effects Transferred to Spin-12 Magic-Angle Spinning Spectra of Solids. *Progress in Nuclear Magnetic Resonance Spectroscopy* **1992**, *24* (5), 435–456. https://doi.org/10.1016/0079-6565(92)80004-Y.
(70) Martineau, C.; Fayon, F.; Legein, C.; Buzaré, J.-Y.; Silly, G.; Massiot, D. Accurate Heteronuclear J-Coupling Measurements in Dilute Spin Systems Using the Multiple-Quantum Filtered J-Resolved Experiment. *Chem. Commun.* **2007**, No. 26, 2720–2722. https://doi.org/10.1039/B703321D.
(71) Latouche, C.; Barone, V. Computational Chemistry Meets Experiments for Explaining the Behavior of Bibenzyl: A Thermochemical and Spectroscopic (Infrared, Raman, and NMR) Investigation. *J. Chem. Theory Comput.* **2014**, *10* (12), 5586–5592. https://doi.org/10.1021/ct500930b.
(72) Bowmaker, G. A.; Healy, P. C. The Characterization of Tetrameric Complexes of Copper(I) Halides with Phosphine and Amine Ligands by Far Infrared Spectroscopy. *Spectrochimica Acta Part A: Molecular Spectroscopy* **1988**, *44* (1), 115–119. https://doi.org/10.1016/0584-8539(88)80267-8.
(73) Attar, S.; Nelson, J. H. Phosphole Complexes of Copper(I) Halides. Investigations of Structure and Bonding by X-Ray Crystallography, Infrared Spectroscopy, and CP/MAS 31P NMR Spectroscopy. *Inorg. Chem.* **1991**, *30*, 4143–4153.

(74) Utrera-Melero, R.; Huitorel, B.; Cordier, M.; Mevellec, J.-Y.; Massuyeau, F.; Latouche, C.; Martineau-Corcos, C.; Perruchas, S. Combining Theory and Experiment to Get Insight into the Amorphous Phase of Luminescent Mechanochromic Copper Iodide Clusters. *Inorg. Chem.* **2020**, *59* (18), 13607–13620. https://doi.org/10.1021/acs.inorgchem.0c01967.

(75) Schlachter, A.; Viau, L.; Fortin, D.; Knauer, L.; Strohmann, C.; Knorr, M.; Harvey, P. D. Control of Structures and Emission Properties of $(CuI)_n$ 2-Methyldithiane Coordination Polymers. *Inorg. Chem.* **2018**, *57* (21), 13564–13576. https://doi.org/10.1021/acs.inorgchem.8b02168.

(76) M. J. Frisch and G. W. Trucks and H. B. Schlegel and G. E. Scuseria and M. A. Robb and J. R. Cheeseman and G. Scalmani and V. Barone and G. A. Petersson and H. Nakatsuji and X. Li and M. Caricato and A. V. Marenich and J. Bloino and B. G. Janesko and R. Gomperts and B. Mennucci and H. P. Hratchian and J. V. Ortiz and A. F. Izmaylov and J. L. Sonnenberg and D. Williams-Young and F. Ding and F. Lipparini and F. Egidi and J. Goings and B. Peng and A. Petrone and T. Henderson and D. Ranasinghe and V. G. Zakrzewski and J. Gao and N. Rega and G. Zheng and W. Liang and M. Hada and M. Ehara and K. Toyota and R. Fukuda and J. Hasegawa and M. Ishida and T. Nakajima and Y. Honda and O. Kitao and H. Nakai and T. Vreven and K. Throssell and Montgomery, {Jr.}, J. A. and J. E. Peralta and F. Ogliaro and M. J. Bearpark and J. J. Heyd and E. N. Brothers and K. N. Kudin and V. N. Staroverov and T. A. Keith and R. Kobayashi and J. Normand and K. Raghavachari and A. P. Rendell and J. C. Burant and S. S. Iyengar and J. Tomasi and M. Cossi and J. M. Millam and M. Klene and C. Adamo and R. Cammi and J. W. Ochterski and R. L. Martin and K. Morokuma and O. Farkas and J. B. Foresman and D. J. Fox. Gaussian 16, Revision A.03, 2016.

(77) De Angelis, F.; Fantacci, S.; Sgamellotti, A.; Cariati, E.; Ugo, R.; Ford, P. C. Electronic Transitions Involved in the Absorption Spectrum and Dual Luminescence of Tetranuclear Cubane $[Cu_4I_4(Pyridine)_4]$ Cluster: A Density Functional Theory/Time-Dependent Density Functional Theory Investigation. *Inorg. Chem.* **2006**, *45* (26), 10576–10584. https://doi.org/10.1021/ic061147f.

For Table of Contents Only

The study of a series of tetranuclear and octanuclear copper iodide clusters coordinated with different phosphine ligands permit to evaluate the effect of the dimerization of the cubane core and the influence of the nature of the ligands on their photophysical properties.